Relativistic tight-binding calculations of x-ray absorption and magnetic circular dichroism at the L_2 and L_3 edges of nickel and iron

N. V. Smith, C. T. Chen, F. Sette, and L. F. Mattheiss
AT&T Bell Laboratories, Murray Hill, New Jersey 07974
(Received 22 January 1992)

The soft-x-ray absorption and magnetic circular dichroism (MCD) cross sections at the L_2 and L_3 core-level edges of Ni and Fe have been calculated using a one-electron tight-binding band-structure approach. The tight-binding scheme is taken from the work of Papaconstantopoulos, supplemented with the inclusion of spin-orbit coupling in the d bands and fully relativistic dipole selection rules. In Ni, a fit to the various L_2 and L_3 intensity ratios can be achieved, but only with values of the d-band spin-orbit parameter ξ and exchange parameter Δ_{ex} at variance with the ground-state band-structure values. For Fe, there is no plausible value of ξ capable of explaining the intensity ratios; also, the predicted substructure within the L_2 and L_3 white lines is not seen in experiment. These failures of the one-electron approach are qualitatively consistent with expected many-body electronic rearrangements associated with core-hole creation. Some discussion is offered on sum rules and on orbital versus spin magnetic moments.

I. INTRODUCTION

The out-of-plane radiation emitted by synchrotron-radiation sources has a high degree of circular polarization. This feature has been exploited recently in several studies of magnetic circular dichroism (MCD) at core-level edges in both soft-x-ray[1] and hard-x-ray[2] absorption. These activities are part of a larger current trend to study magnetic properties of solids using synchrotron-radiation-based techniques: linear dichroism,[3] magnetic diffraction and scattering,[4] and spin-polarized photoemission.[5]

The *primary* aim of this paper is to report the results of a tight-binding analysis of recent high-resolution measurements of the soft-x-ray absorption and MCD at the $L_2(2p_{1/2}\rightarrow 3d)$ and $L_3(2p_{3/2}\rightarrow 3d)$ core-level edges of Ni and Fe. The starting point of our analysis is the tight-binding representation of Ni and Fe given in the work of Papaconstantopoulos.[6] To this basic representation we have added spin-orbit coupling within the valence d bands and relativistic dipole selection rules. These additions are spelled out in Secs. II and III A in some detail since it is the *secondary* aim of this paper to provide a self-contained supplement to the book by Papaconstantopoulos which would permit interested experimentalists to perform similar calculations. Further calculational details are provided in Sec. III. The results, discussion, and conclusions are presented in Secs. IV and V.

Our tight-binding analysis may be viewed as an attempt to determine the limits of a one-electron band-structure interpretation. It has been anticipated in previous papers[7] that tight-binding analyses could expose the failure of the one-electron band-structure approach and confirm the need for many-body corrections such as edge singularities,[8] Fano line shapes,[9] and valence self-energies.[10] Our results do in fact demonstrate the need for such corrections. A preliminary communication on this work has already been published.[11]

II. RELATIVISTIC DIPOLE SELECTION RULES

A. Basis states

In calculating soft-x-ray core-level absorption and MCD spectra in Ni and Fe, it is essential to take relativistic effects into account. We may distinguish, however, two approaches. In the first approach, only the core states are treated relativistically (spin-orbit-split levels). In the context of core-level MCD in Ni, this approach has been advanced by Erskine and Stern using a simplified exchange-split representation of the $3d$ valence band.[12] We shall refer to this approach as the Erskine-Stern model, and it is described below in Sec. II B. The second approach incorporates spin-orbit splitting into both the core and valence levels. This fully relativistic model is described in Sec. II C.

The detailed band calculations of this paper use the tight-binding or linear combination of atomic orbitals (LCAO) method of Slater and Koster,[13] as elaborated and parametrized in the recent book by Papaconstantopoulos.[6] The basis states appropriate to a relativistic treatment are expressed in terms of the standard Slater-Koster basis states in Table I.

B. Erskine-Stern model

The simplest available model of core-level x-ray-absorption cross sections and associated MCD is that of Erskine and Stern.[12] They point out that for Ni the unoccupied $3d$ states lie in a narrow energy range just above the Fermi level E_F and (in the absence of spin-orbit interaction) are exclusively of $\downarrow$ spin. We therefore need consider only the set of squared-dipole-matrix elements shown in Table II. The quantities A, B, and C of Table II are defined as

$$A = |\langle Y_{2\pm2}|(x\pm iy)/r|Y_{1\pm1}\rangle|^2 R^2 ,$$
$$B = |\langle Y_{2\pm1}|(x\pm iy)/r|Y_{10}\rangle|^2 R^2 , \quad (1)$$
$$C = |\langle Y_{20}|(x\mp iy)/r|Y_{1\pm1}\rangle|^2 R^2 ,$$

where R is the standard integral,

$$R = \int r^2 R_p(r) R_d(r) dr , \quad (2)$$

and where $R_p(r)$ and $R_d(r)$ are the $2p$ and $3d$ radial wave functions. Actually, A, B, and C reduce to $\frac{4}{5}R^2$, $\frac{2}{5}R^2$, and $\frac{2}{15}R^2$, respectively, but we shall retain them as independent parameters in order to make contact with the results of Ref. 12. Summing over the entire manifold of unoccupied $d^\downarrow$ states, one obtains for the total cross section $(\sigma_+ + \sigma_-)$ and the MCD cross section $(\sigma_+ - \sigma_-)$ the expressions

$$L_3(p_{3/2}\rightarrow d^\downarrow)\begin{cases}\sigma_+ + \sigma_- = \frac{4}{3}A + \frac{4}{3}B + \frac{4}{3}C, \\ \sigma_+ - \sigma_- = -\frac{2}{3}A + \frac{2}{3}C ,\end{cases}$$
$$L_2(p_{1/2}\rightarrow d^\downarrow)\begin{cases}\sigma_+ + \sigma_- = \frac{2}{3}A + \frac{2}{3}B + \frac{2}{3}C, \\ \sigma_+ - \sigma_- = \frac{2}{3}A - \frac{2}{3}C .\end{cases} \quad (3)$$

A tacit assumption of this model is that the final states may be treated incoherently in the summation. Since a Brillouin-zone integral is involved, such an assumption is entirely reasonable. Erskine and Stern apply a weighting of $\frac{1}{2}$,1,0 to the A,B,C terms of Eq. (3) based on an inspec-

TABLE I. Relativistic basis states $|j,m_j\rangle$ expressed in terms of spherical harmonics $Y^\uparrow_{lm}$ and $Y^\downarrow_{lm}$ and the standard basis states of the Slater-Koster LCAO interpolation method.

	Spherical harmonic	Slater-Koster LCAO
$\|\frac{1}{2},\frac{1}{2}\rangle$	$Y^\uparrow_{00}$	$s^\uparrow$
$\|\frac{1}{2},-\frac{1}{2}\rangle$	$Y^\downarrow_{00}$	$s^\downarrow$
$\|\frac{1}{2},\frac{1}{2}\rangle$	$-\frac{1}{\sqrt{3}}Y^\uparrow_{10}+\frac{\sqrt{2}}{\sqrt{3}}Y^\downarrow_{11}$	$-\frac{1}{\sqrt{3}}p_z^\uparrow-\frac{1}{\sqrt{3}}(p_x^\downarrow+ip_y^\downarrow)$
$\|\frac{1}{2},-\frac{1}{2}\rangle$	$-\frac{\sqrt{2}}{\sqrt{3}}Y^\uparrow_{1-1}+\frac{1}{\sqrt{3}}Y^\downarrow_{10}$	$-\frac{1}{\sqrt{3}}(p_x^\uparrow-ip_y^\uparrow)+\frac{1}{\sqrt{3}}p_z^\downarrow$
$\|\frac{3}{2},\frac{3}{2}\rangle$	$Y^\uparrow_{11}$	$-\frac{1}{\sqrt{2}}(p_x^\uparrow+ip_y^\uparrow)$
$\|\frac{3}{2},\frac{1}{2}\rangle$	$\frac{\sqrt{2}}{\sqrt{3}}Y^\uparrow_{10}+\frac{1}{\sqrt{3}}Y^\downarrow_{11}$	$\frac{\sqrt{2}}{\sqrt{3}}p_z^\uparrow-\frac{1}{\sqrt{6}}(p_x^\downarrow+ip_y^\downarrow)$
$\|\frac{3}{2},-\frac{1}{2}\rangle$	$\frac{1}{\sqrt{3}}Y^\uparrow_{1-1}+\frac{\sqrt{2}}{\sqrt{3}}Y^\downarrow_{10}$	$\frac{1}{\sqrt{6}}(p_x^\uparrow-ip_y^\uparrow)+\frac{\sqrt{2}}{\sqrt{3}}p_z^\downarrow$
$\|\frac{3}{2},-\frac{3}{2}\rangle$	$Y^\downarrow_{1-1}$	$\frac{1}{\sqrt{2}}(p_x^\downarrow-ip_y^\downarrow)$
$\|\frac{3}{3},\frac{3}{2}\rangle$	$-\frac{\sqrt{5}}{5}Y^\uparrow_{21}+\frac{2\sqrt{5}}{5}Y^\downarrow_{22}$	$\frac{1}{\sqrt{10}}(d^\uparrow_{zx}+id^\uparrow_{yz})+\frac{2}{\sqrt{10}}(d^\downarrow_{x^2-y^2}+id^\downarrow_{xy})$
$\|\frac{3}{2},\frac{1}{2}\rangle$	$-\frac{\sqrt{10}}{5}Y^\uparrow_{20}+\frac{\sqrt{15}}{5}Y^\downarrow_{21}$	$-\frac{2}{\sqrt{10}}d^\uparrow_{3z^2-r^2}-\frac{3}{\sqrt{30}}(d^\downarrow_{zx}+id^\downarrow_{yz})$
$\|\frac{3}{2},-\frac{1}{2}\rangle$	$-\frac{\sqrt{15}}{5}Y^\uparrow_{2-1}+\frac{\sqrt{10}}{5}Y^\downarrow_{20}$	$-\frac{3}{\sqrt{30}}(d^\uparrow_{zx}-id^\uparrow_{yz})+\frac{2}{\sqrt{10}}d^\downarrow_{3z^2-r^2}$
$\|\frac{3}{2},-\frac{3}{2}\rangle$	$-\frac{2\sqrt{5}}{5}Y^\uparrow_{2-2}+\frac{\sqrt{5}}{5}Y^\downarrow_{2-1}$	$-\frac{2}{\sqrt{10}}(d^\uparrow_{x^2-y^2}-id^\uparrow_{xy})+\frac{1}{\sqrt{10}}(d^\downarrow_{zx}-id^\downarrow_{yz})$
$\|\frac{5}{2},\frac{5}{2}\rangle$	$Y^\uparrow_{22}$	$\frac{1}{\sqrt{2}}(d^\uparrow_{x^2-y^2}+id^\uparrow_{xy})$
$\|\frac{5}{2},\frac{3}{2}\rangle$	$\frac{2\sqrt{5}}{5}Y^\uparrow_{21}+\frac{\sqrt{5}}{5}Y^\downarrow_{22}$	$-\frac{2}{\sqrt{10}}(d^\uparrow_{xz}+id^\uparrow_{yz})+\frac{1}{\sqrt{10}}(d^\downarrow_{x^2-y^2}+id^\downarrow_{xy})$
$\|\frac{5}{2},\frac{1}{2}\rangle$	$\frac{\sqrt{15}}{5}Y^\uparrow_{20}+\frac{\sqrt{10}}{5}Y^\downarrow_{21}$	$\frac{3}{\sqrt{15}}d^\uparrow_{3z^2-r^2}-\frac{1}{\sqrt{5}}(d^\downarrow_{zx}+id^\downarrow_{yz})$
$\|\frac{5}{2},-\frac{1}{2}\rangle$	$\frac{\sqrt{10}}{5}Y^\uparrow_{2-1}+\frac{\sqrt{15}}{5}Y^\downarrow_{20}$	$\frac{1}{\sqrt{5}}(d^\uparrow_{zx}-id^\uparrow_{yz})+\frac{3}{\sqrt{15}}d^\downarrow_{3z^2-r^2}$
$\|\frac{5}{2},-\frac{3}{2}\rangle$	$\frac{\sqrt{5}}{5}Y^\uparrow_{2-2}+\frac{2\sqrt{5}}{5}Y^\downarrow_{2-1}$	$\frac{1}{\sqrt{10}}(d^\uparrow_{x^2-y^2}-id^\uparrow_{xy})+\frac{2}{\sqrt{10}}(d^\downarrow_{zx}-id^\downarrow_{yz})$
$\|\frac{5}{2},-\frac{5}{2}\rangle$	$Y^\downarrow_{2-2}$	$\frac{1}{\sqrt{2}}(d^\downarrow_{x^2-y^2}-id^\downarrow_{xy})$

TABLE II. Dipole matrix elements (squared) for $p \rightarrow d$ optical transitions in the Erskine-Stern model of MCD.

	$p_{3/2}$				$p_{1/2}$	
	$\lvert\frac{3}{2},\frac{3}{2}\rangle$	$\lvert\frac{3}{2},\frac{1}{2}\rangle$	$\lvert\frac{3}{2},-\frac{1}{2}\rangle$	$\lvert\frac{3}{2},-\frac{3}{2}\rangle$	$\lvert\frac{1}{2},\frac{1}{2}\rangle$	$\lvert\frac{1}{2},-\frac{1}{2}\rangle$
			$\sigma_+ = \lvert\langle\lvert(x+iy)/r\rvert\rangle\rvert^2$			
$Y^{\downarrow}_{22}$	0	$\frac{1}{3}A$	0	0	$\frac{2}{3}A$	0
$Y^{\downarrow}_{21}$	0	0	$\frac{2}{3}B$	0	0	$\frac{1}{3}B$
$Y^{\downarrow}_{20}$	0	0	0	C	0	0
$Y^{\downarrow}_{2-1}$	0	0	0	0	0	0
$Y^{\downarrow}_{2-2}$	0	0	0	0	0	0
			$\sigma_- = \lvert\langle\lvert(x-iy)/r\rvert\rangle\rvert^2$			
$Y^{\downarrow}_{22}$	0	0	0	0	0	0
$Y^{\downarrow}_{21}$	0	0	0	0	0	0
$Y^{\downarrow}_{20}$	0	$\frac{1}{3}C$	0	0	$\frac{2}{3}C$	0
$Y^{\downarrow}_{2-1}$	0	0	$\frac{2}{3}B$	0	0	$\frac{1}{3}B$
$Y^{\downarrow}_{2-2}$	0	0	0	A	0	0

tion of a published band calculation.[14] No matter how the A,B,C terms are weighted, however, the model predicts that the $L_3(p_{3/2})$ to $L_2(p_{1/2})$ ratio should be 2:1 for the total cross section and -1:1 for the MCD cross section.

C. Fully relativistic model

The inflexibility of the Erskine-Stern model is a consequence of its perfect symmetry between $Y^{\downarrow}_{22}$ and $Y^{\downarrow}_{2-2}$ and between $Y^{\downarrow}_{21}$ and $Y^{\downarrow}_{2-1}$ wave-function character. This symmetry is removed if the final states are treated relativistically, that is to say, if valence-band spin-orbit coupling is included. The physics here was anticipated in a 1949 paper by Mott.[15] Spin-orbit splitting will enhance $j=\frac{5}{2}$ over $j=\frac{3}{2}$ character near the top of the valence d band, and this will favor the intensity of the L_3 over the L_2 absorption edge.

In Table III we display the dipole matrix elements appropriate to optical transitions between spin-orbit-split p levels and spin-orbit-split d levels. Mott's hypothesis may be divined from Tables II and III by noting that valence spin-orbit interaction will enrich the top of the d band with $\lvert\frac{5}{2},-\frac{5}{2}\rangle$ (i.e., $Y^{\downarrow}_{2-2}$) character.

It should be stressed that it is straightforward (although tedious) to extract all the results of this section from standard texts.[16] They are included here as part of the secondary aim of this paper, which is to provide a useful self-contained supplement to Ref. 6.

III. CALCULATION METHODS

A. Band structures

We take as our starting point for the band structures of Ni and Fe the tight-binding representations included in the work of Papaconstantopoulos.[6] Specifically, we take the "three-center nonorthogonal" parameter sets listed on pp. 111 and 115 for Ni and pp. 95 and 99 for Fe. Spin-orbit coupling within the $3d$ valence band is incorporated by doubling the 9×9 tight-binding Hamiltonian:[17]

$$H=\begin{bmatrix} H^{\uparrow}_{cc} & H^{\uparrow}_{cd} & 0 & 0 \\ H^{\uparrow}_{dc} & H^{\uparrow}_{dd}+\xi M & 0 & \xi N \\ 0 & 0 & H^{\downarrow}_{cc} & H^{\downarrow}_{cd} \\ 0 & -\xi N^* & H^{\downarrow}_{dc} & H^{\downarrow}_{cc}+\xi M^* \end{bmatrix}. \tag{4}$$

ξ is the spin-orbit parameter, and the matrices M and N are given by

$$M=\frac{i}{2}\begin{bmatrix} 0 & ss' & -sc' & 2c & 0 \\ -ss' & 0 & c & -sc' & -3^{1/2}sc' \\ sc' & -c & 0 & -ss' & 3^{1/2}ss' \\ -2c & sc' & ss' & 0 & 0 \\ 0 & 3^{1/2}sc' & -3^{1/2}ss' & 0 & 0 \end{bmatrix}, \tag{5}$$

$$N=\frac{1}{2}\begin{vmatrix} 0 & c'+ics' & s'-icc' & -2is & 0 \\ -(c'+ics') & 0 & -is & s'-icc' & 3^{1/2}(s'-icc') \\ -(s'-icc') & is & 0 & -(c'+ics') & 3^{1/2}(c'+ics') \\ 2is & -(s'-icc') & (c'+ics') & 0 & 0 \\ 0 & -3^{1/2}(s'-icc') & -3^{1/2}(c'+ics') & 0 & 0 \end{vmatrix}, \tag{6}$$

where $c\equiv\cos\theta$, $s\equiv\sin\theta$, $c'\equiv\cos\phi$, $s'\equiv\sin\phi$, and θ,ϕ are the polar coordinates of the direction of spin quantization. These are standard expressions,[18] but are included here as part of the secondary aim of this paper.

There are two main distinctions between the ferromagnetic band structures of Ni and Fe. First, the exchange splitting Δ_{ex} is much smaller in Ni ($\sim$0.6 eV) than in Fe ($\sim$2.0 eV). Second, the majority-spin d bands in Ni are totally occupied; i.e., there are no $\uparrow$ spin holes. In Fe, on the other hand, there is an appreciable number of $\uparrow$ spin holes. This latter point will assume considerable importance in the discussion in Sec. V below.

Variations of the exchange parameter Δ_{ex} were handled as follows. Papaconstantopoulos presents separate parameter sets for the up- and down-spin systems. The main distinction between these parameter sets resides in the difference between the mean diagonal d-orbital energies of the up- and down-spin systems, and this defines Δ_{ex}. The remaining fitting parameters (more than 60 in all) display small differences between the up- and down-spin systems. The paramagnetic case was simulated by simply averaging the up- and down-spin parameter sets. Nonzero Δ_{ex} parameter sets were then generated by linear interpolation or extrapolation.

TABLE III. Dipole matrix elements (squared) for $p\rightarrow d$ optical transitions in the fully relativistic model.

		$p_{3/2}$				$p_{1/2}$	
		$\lvert\frac{3}{2},\frac{3}{2}\rangle$	$\lvert\frac{3}{2},\frac{1}{2}\rangle$	$\lvert\frac{3}{2},-\frac{1}{2}\rangle$	$\lvert\frac{3}{2},-\frac{3}{2}\rangle$	$\lvert\frac{1}{2},\frac{1}{2}\rangle$	$\lvert\frac{1}{2},-\frac{1}{2}\rangle$
				$\sigma_+=\lvert\langle\lvert(x+iy)/r\rvert\rangle\rvert^2$			
$d_{5/2}$	$\langle\frac{5}{2},\frac{5}{2}\rvert$	$\frac{4}{5}R^2$	0	0	0	0	0
	$\langle\frac{5}{2},\frac{3}{2}\rvert$	0	$\frac{12}{25}R^2$	0	0	0	0
	$\langle\frac{5}{2},\frac{1}{2}\rvert$	0	0	$\frac{6}{25}R^2$	0	0	0
	$\langle\frac{5}{2},-\frac{1}{2}\rvert$	0	0	0	$\frac{2}{25}R^2$	0	0
	$\langle\frac{5}{2},-\frac{3}{2}\rvert$	0	0	0	0	0	0
	$\langle\frac{5}{2},-\frac{5}{2}\rvert$	0	0	0	0	0	0
$d_{3/2}$	$\langle\frac{3}{2},\frac{3}{2}\rvert$	0	$\frac{12}{225}R^2$	0	0	$\frac{2}{3}R^2$	0
	$\langle\frac{3}{2},\frac{1}{2}\rvert$	0	0	$\frac{16}{225}R^2$	0	0	$\frac{2}{9}R^2$
	$\langle\frac{3}{2},-\frac{1}{2}\rvert$	0	0	0	$\frac{12}{225}R^2$	0	0
	$\langle\frac{3}{2},-\frac{3}{2}\rvert$	0	0	0	0	0	0
				$\sigma_-=\lvert\langle\lvert(x-iy)/r\rvert\rangle\rvert^2$			
$d_{5/2}$	$\langle\frac{5}{2},\frac{5}{2}\rvert$	0	0	0	0	0	0
	$\langle\frac{5}{2},\frac{3}{2}\rvert$	0	0	0	0	0	0
	$\langle\frac{5}{2},\frac{1}{2}\rvert$	$\frac{2}{25}R^2$	0	0	0	0	0
	$\langle\frac{5}{2},-\frac{1}{2}\rvert$	0	$\frac{6}{25}R^2$	0	0	0	0
	$\langle\frac{5}{2},-\frac{3}{2}\rvert$	0	0	$\frac{12}{25}R^2$	0	0	0
	$\langle\frac{5}{2},-\frac{5}{2}\rvert$	0	0	0	$\frac{4}{5}R^2$	0	0
$d_{3/2}$	$\langle\frac{3}{2},\frac{3}{2}\rvert$	0	0	0	0	0	0
	$\langle\frac{3}{2},\frac{1}{2}\rvert$	$\frac{12}{225}R^2$	0	0	0	0	0
	$\langle\frac{3}{2},-\frac{1}{2}\rvert$	0	$\frac{16}{225}R^2$	0	0	$\frac{2}{9}R^2$	0
	$\langle\frac{3}{2},-\frac{3}{2}\rvert$	0	0	$\frac{12}{225}R^2$	0	0	$\frac{2}{3}R^2$

B. Cross sections

Computation of the absorption of circularly polarized x rays by a core state $|c\rangle$ at energy E_c involves Brillouin-zone (BZ) integrals of the form

$$\sigma_{\pm}(\hbar\omega) \propto \sum_n \int_{\mathrm{BZ}} d\mathbf{k} |\langle \mathbf{k},n|x \pm iy|c\rangle|^2 \times \delta(E_{\mathbf{k},n} - E_c - \hbar\omega) , \quad (7)$$

where the summation is over the band index n appropriate to band states $|\mathbf{k},n\rangle$ of energy $E_{\mathbf{k},n}$. The total x-ray-absorption cross section is given by $(\sigma_+ + \sigma_-)$ and the MCD cross section by $(\sigma_+ - \sigma_-)$. The way in which integrals of this kind can be expressed as l-projected densities of states has been presented elsewhere.[9,19]

The zone integral was performed by calculating energies and eigenvectors at points on a cubic mesh in $\mathbf{k}$ space and then using trilinear interpolation on a denser mesh. In the simultaneous presence of spin-orbit coupling and exchange interaction, the usual $\frac{1}{48}$th irreducible wedges of the BZ are no longer equivalent. This was accommodated by sampling the BZ over a sufficiently large volume, even at the expense of some redundant counting. The typical number of diagonalizations was ~ 5000, and the corresponding number of interpolated $\mathbf{k}$ points sampled was $\sim 10^6$. It is the computational speed of the tight-binding approach which permits us to perform numerous numerical experiments to quantify the influence of key parameters such as ξ and Δ_{ex}. This is in contrast with the more rigorous first-principles calculations which have already been applied to this kind of problem.[20,21]

C. Magnetic anisotropy

A consequence of the lower symmetry in the sampling of the BZ is that the MCD spectrum will vary with the chosen direction of spin quantization, (θ,ϕ) in Eq. (5) above. We have tested this expectation by calculating the MCD spectrum with (θ,ϕ) values corresponding to the [111], [001], and [110] directions in Ni. In principle, one could perform experiments in which the magnetization direction and photon incidence direction are normal to (111), (001), and (110) surfaces of single-crystal samples and then examine the differences in the MCD spectrum. We find that such differences are very small, essentially at the noise level of the present calculations. We conclude that it would not be fruitful to search for such anisotropies experimentally at this time.

IV. NICKEL: RESULTS AND DISCUSSION

A. Calculated spectra

L_2 and L_3 absorption $(\sigma_+ + \sigma_-)$ and MCD $(\sigma_+ - \sigma_-)$ spectra computed by the present tight-binding model for Ni are displayed in Fig. 1 over the valence-band region without regard for the Pauli exclusion principle. Because of the exclusion principle, only that part of the spectrum above the Fermi level E_F is, of course, observable. Two cases are considered in Fig. 1: $\xi = 0$ and $\xi \neq 0$.

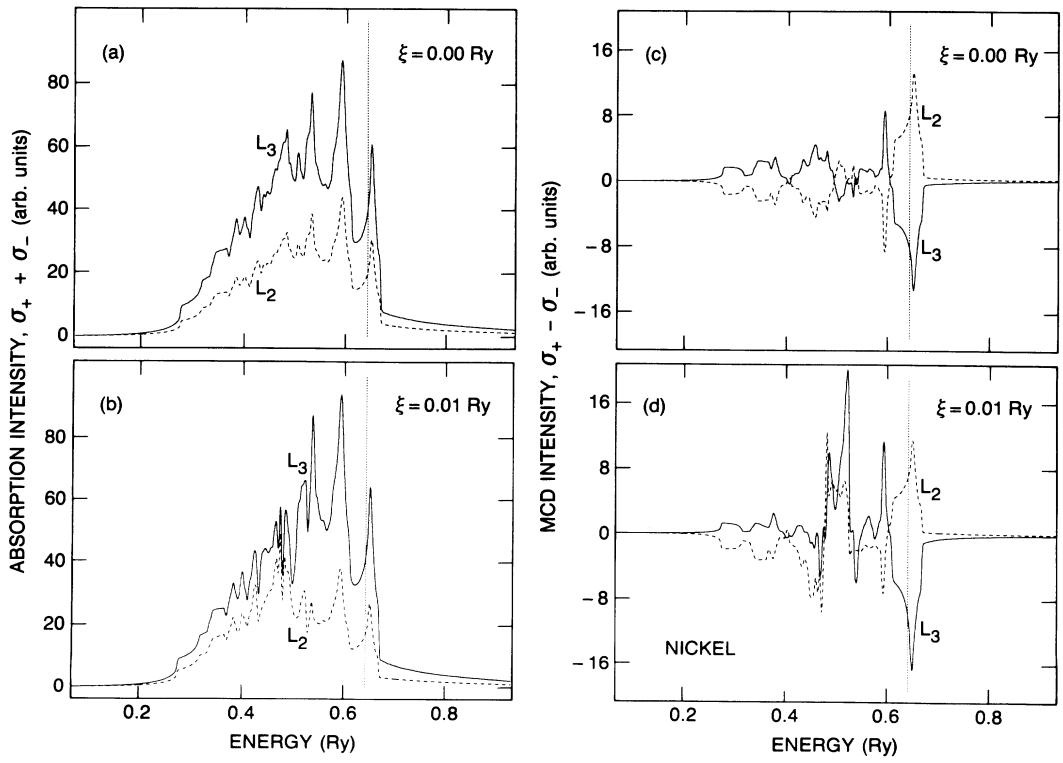

FIG. 1. Calculated L_3 (solid curves) and L_2 (dashed curves) spectra for Ni without regard for the exclusion principle. Only that part above E_F is observable experimentally. Panels (a) and (b) show the total absorption cross section $(\sigma_+ + \sigma_-)$ for $\xi = 0$ and 0.01 Ry, respectively; panels (c) and (d) are the corresponding $(\sigma_+ - \sigma_-)$ MCD cross sections. The exchange parameter is $\Delta_{\mathrm{ex}} = 0.056$ Ry.

In the $\xi=0$ case, the L_3- to L_2-intensity ratio is 2:1 in the $\sigma_+ + \sigma_-$ spectrum and -1:1 in $\sigma_+ - \sigma_-$ *at each energy value within the valence band.* This is expected and is in accord with the Erskine-Stern model of Sec. II C. In the presence of a d spin-orbit interaction ($\xi \neq 0$), however, this point-by-point correspondence is removed. States at the top of the d band are richer in $j=\frac{5}{2}$ character, and this enhances the L_3 over the L_2 intensity.[15] In Sec. IV C below, we exploit this phenomenon to extract an effective value of ξ.

B. Sum-rule considerations

The removal by spin-orbit splitting of the point-by-point -1:1 ratio in the MCD spectrum lends itself to a digression on the subject of sum rules. There is a very fundamental sum rule for magneto-optical absorption[22] which requires that

$$\int_0^\infty [\sigma_+(\omega) - \sigma_-(\omega)] d\omega = 0 \ . \tag{8}$$

Our experimental MCD observation of the L_3- to L_2-intensity ratios very different from -1:1 might, at first sight, appear to violate this sum rule. The resolution of such an apparent violation has been considered earlier.[23] In the presence of the exclusion principle, sum rules cannot be applied in a piecewise fashion over restricted frequency ranges.

If the exclusion principle is ignored, a piecewise application of the sum rules *is* valid. This can be sensed by inspection of Figs. 1(c) and 1(d) for Ni as well as the corresponding figures for Fe in Sec. V below. Integrating over the entire valence band, Eq. (8) is obeyed. In the presence of the exclusion principle, however, we observe only that part of the spectrum above E_F, and the integral of Eq. (8) applied over this very restricted frequency range is definitely *not* zero when $\xi \neq 0$. As argued elsewhere,[23] this imbalance must be compensated in other frequency ranges.

C. Comparison with experiment

In the case of Ni, we have performed numerous numerical experiments in order to arrive at an "optimal simulation" of the experimental spectra. The two governing parameters are ξ and Δ_{ex}. Our procedure was to examine certain intensity ratios. It has proved useful to distinguish between *intraspectral* ratios, that is to say, the L_3- to L_2-intensity ratios within the individual absorption ($\sigma_+ + \sigma_-$) and MCD ($\sigma_+ - \sigma_-$) spectra, and *interspectral* ratios, that is to say, the between-spectra intensity ratios $(\sigma_+ - \sigma_-)/(\sigma_+ + \sigma_-)$ for the L_3,L_2 white lines. The latter are subject to more uncertainty since they depend on a calibration of the degree of circular polarization in the incident x-ray beam and on the degree of sample magnetization.

The L_3- to L_2-intensity ratio in both ($\sigma_+ + \sigma_-$) and ($\sigma_+ - \sigma_-$) depends almost exclusively on ξ and only weakly on Δ_{ex}. This is seen in Fig. 2(a), which plots the calculated L_3- to L_2-intensity ratio versus Δ_{ex} for various trial values of ξ. Agreement with experiment [indicated in Fig. 2(a) by the toned horizontal strips] can be achieved simultaneously for both ($\sigma_+ + \sigma_-$) and ($\sigma_+ - \sigma_-$). We choose as our optimal value $\xi = 0.0095 \pm 0.0005$ Ry. This value is considerably larger than the one-electron band-structure value[14] (0.0067 Ry) and the experimental atomic value[18,24] (0.0055 Ry). It is marginally larger than the theoretical Herman-Skillman atomic value[25] (0.0081 Ry).

By contrast, the intensity ratio of $(\sigma_+ - \sigma_-)/(\sigma_+ + \sigma_-)$ depends primarily on Δ_{ex} and only slightly on ξ, as illustrated in Fig. 2(b). The low experimental values for the $(\sigma_+ - \sigma_0)/(\sigma_+ + \sigma_-)$ ratio (20±4% for L_3 and 12.5±2.5% for L_2) imply $\Delta_{ex} = 0.025 \pm 0.010$ Ry for the exchange splitting. This value is much lower than typical one-electron band-structure values.[6,14] It is, however, remarkably close to the experimental values obtained from angle-resolved photoemission[26] (0.019–0.023 Ry). This closeness has been offered as potential evidence for the high localization of a Ni $3d$ valence hole.[11]

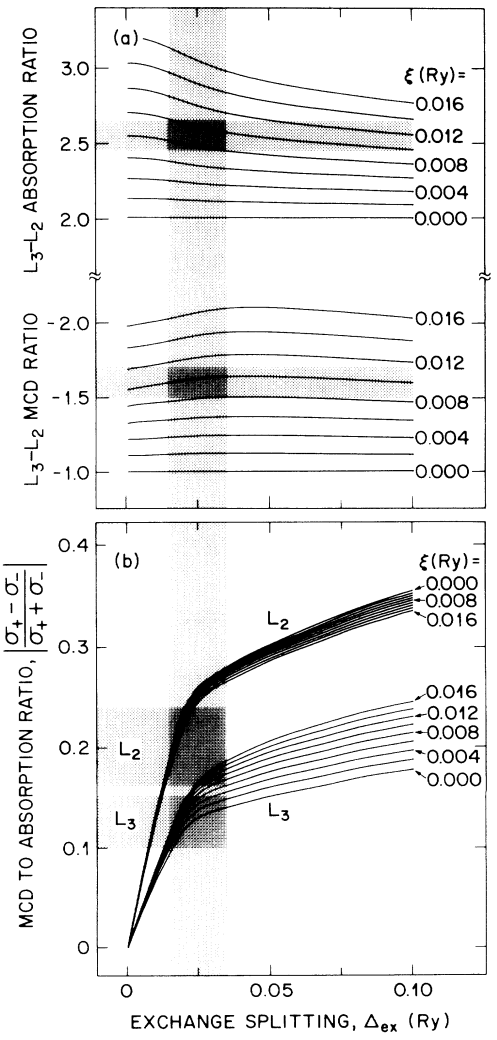

FIG. 2. Calculated intensity ratios of the L_2 and L_3 "white lines" of Ni as a function of the two key parameters ξ and Δ_{ex}: (a) *intraspectral* L_3 to L_2-intensity ratios and (b) *interspectral* ratios $(\sigma_+ - \sigma_-)/(\sigma_+ + \sigma_-)$ for the individual L_2 and L_3 lines. Details of line-shape analysis are given in the text.

D. Line-shape considerations

From the numerical experiments described above, we arrive at the values $\xi=0.0095$ Ry and $\Delta_{ex}=0.025$ Ry, which have been used to generate an "optimal simulation" of the experimental spectra. The precise numbers depend to some extent on the method of line-shape analysis. These details are now spelled out.

The L_2 line is wider than the L_3 line because the decay of a $p_{1/2}$ core hole has a channel (the super-Coster-Kronig process $p_{1/2}\rightarrow p_{3/2}$) not available to a $p_{3/2}$ core hole. The measured white lines were fitted by convolving the calculated spectra with Voigt functions. Our optimal simulation is shown in Fig. 3. The parameters used were 0.8 eV Gaussian full width at half maximum (FWHM) and 0.6 and 1.4 eV Lorentzian FWHM for the L_3 and L_2 white lines, respectively. The value of the L_2,L_3 core-level spin-orbit splitting was fitted to experiment.

E. Discussion

From the above comparisons, we conclude for Ni that one-electron band theory fails—or rather that it can be rescued only by invoking effective values for $\xi(\Delta_{ex})$ larger (smaller) than the ground-state values. Qualitatively speaking, the directions of these discrepancies are consistent with many-body dynamical expectations. On creation of the core hole, the $3d$ valence electrons will see a stronger attractive core potential, and the spatial extent of their orbitals will contract. Consequently, relativistic effects (e.g., spin-orbit splitting) will be stronger, and exchange interaction among neighbors will be weaker.

The feature B (B') in the L_3 (L_2) MCD spectrum of Fig. 3(b) which appears about 4 eV above the main white lines constitutes further evidence of correlation effects. This was attributed initially,[1] in one-electron band-structure terms, to hybridization of d-like character into plane-wave-type states above the nominal top of the Ni $3d$ band. The absence of such a feature in our present calculations indicates that such one-electron interpretations can be safely abandoned. By contrast, feature A (A') in the absorption spectrum ($\sigma_+ + \sigma_-$) of Fig. 3(a) *is* reproduced by our one-electron calculations and those of others.[27] We now propose that the B (B') feature represents a shake-up or shake-off phenomenon analogous to the "6-eV" hole-hole correlation satellite in photoemission.[28–32] The 6-eV satellite is known both theoretically[28] and experimentally[33] to be spin polarized, and so it is provocative that the B (B') feature appears prominently in the MCD spectrum, but is imperceptible in the total absorption spectrum. This many-body feature has recently been reproduced in theoretical calculations by Jo and Sawatsky.[34]

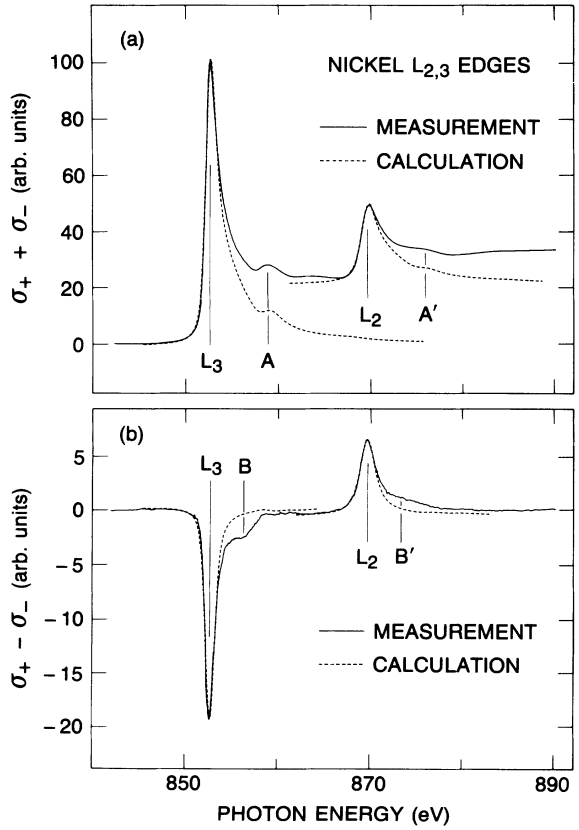

FIG. 3. Comparison for Ni between experimental soft-x-ray spectra (solid curves) and an optimal tight-binding simulation (dashed curves) of the L_3 and L_2 white lines: (a) the total absorption ($\sigma_+ + \sigma_-$) and (b) the magnetic circular dichroism ($\sigma_+ - \sigma_-$). The experimental MCD spectrum shown here has been magnified by a factor of 1.85 to account for incomplete photon polarization and sample magnetization.

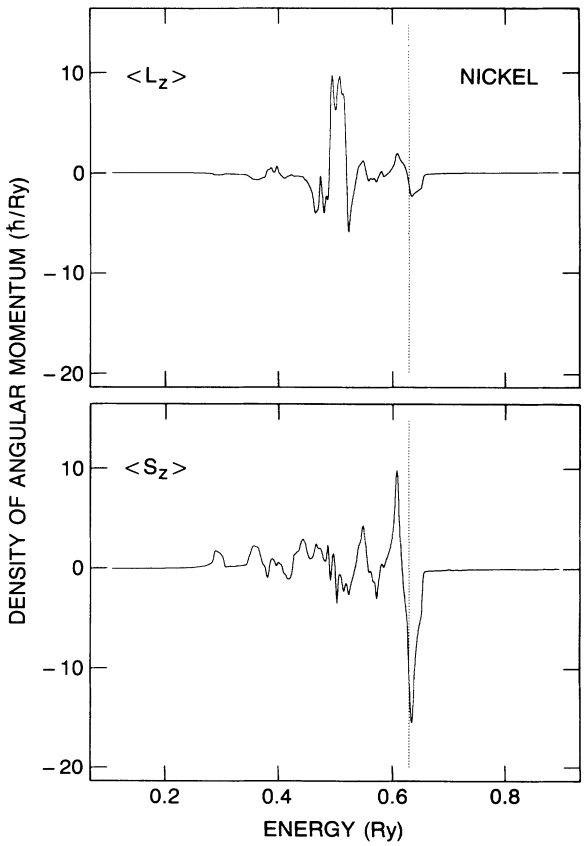

FIG. 4. Calculated spectra for the expectation values $\langle L_z \rangle$ and $\langle S_z \rangle$ of the orbital and spin angular momentum over the d band of Ni for the "optimal simulation" discussed in the text. The integrated orbital and spin magnetic moments per atom are $0.05\mu_B$ and $0.52\mu_B$, respectively.

F. Orbital versus spin magnetic moment

The inclusion of spin-orbit splitting into the $3d$ valence bands of Ni and Fe implies a significant orbital contribution to the magnetic moment per atom. The ratio of orbital to spin magnetic moment continues to be a matter of debate. We show in Fig. 4 the calculated spectra across the Ni valence band for $\langle L_z \rangle$ and $\langle S_z \rangle$ using our optimal simulation.

The magnetic moment is given by $(\langle L_z \rangle + 2\langle S_z \rangle)\mu_B$, where μ_B is the Bohr magneton. Our optimal simulation for Ni yields values of $0.05\mu_B$ and $0.5\mu_B$, respectively, for the integrated orbital and spin magnetic moment per atom. These results are in general agreement with other experimental and theoretical estimates.[34,35] However, this agreement has to be viewed with caution in light of the general breakdown of the one-electron approach.

V. IRON: RESULTS AND DISCUSSION

A. Calculated spectra

Our calculated absorption and MCD spectra for Fe are displayed in Fig. 5, once again without regard for the exclusion principle. The main differences with Ni (see Fig. 1) are twofold: First, Fe has two fewer valence electrons, and so the portion of the d band lying above E_F is wider and richer in structure; second, Fe forms with the bcc rather than the fcc structure. The larger unfilled d bandwidth in Fe offers the possibility of more dramatic changes as we go from the $\xi=0$ to the $\xi\neq 0$ case. Note especially the changes in the calculated MCD spectrum. For the $\xi\neq 0$ case, the L_3 MCD spectrum is predicted to be distinctly positive just above threshold, whereas there is no strong negative counterpart in the L_2 MCD at threshold. This difference is a direct consequence of the existence of ↑ holes in the Fe $3d$ valence band.

B. Comparison with experiment

Our experimental data for the total absorption and MCD at the $L_{2,3}$ edges in Fe are shown in Fig. 6. It is evident at once that there is qualitative disagreement with the one-electron band picture. The experimental spectra consist of featureless white lines. They show none of the substructure predicted by one-electron band theory, even though the observation of such substructure would be well within the resolution capability of the monochromator. In particular, we find no positive excursion of the MCD signal at the L_3 threshold.

The *intraspectral* L_3- to L_2-intensity ratio in the $(\sigma_+ + \sigma_-)$ spectrum is found experimentally to be 2.6 ± 0.1, significantly larger than the 2:1 ratio of the Erskine-Stern model. In principle, we can simulate this ratio with an appropriate value for ξ. The actual value is $\xi=0.015\pm0.001$ Ry. This is considerably larger than the atomic value $\xi=0.0035$ Ry or the first-principles band structure value $\xi=0.0043$ Ry quoted by Singh, Wang, and Calloway[36] The Herman-Skillman[25] value is

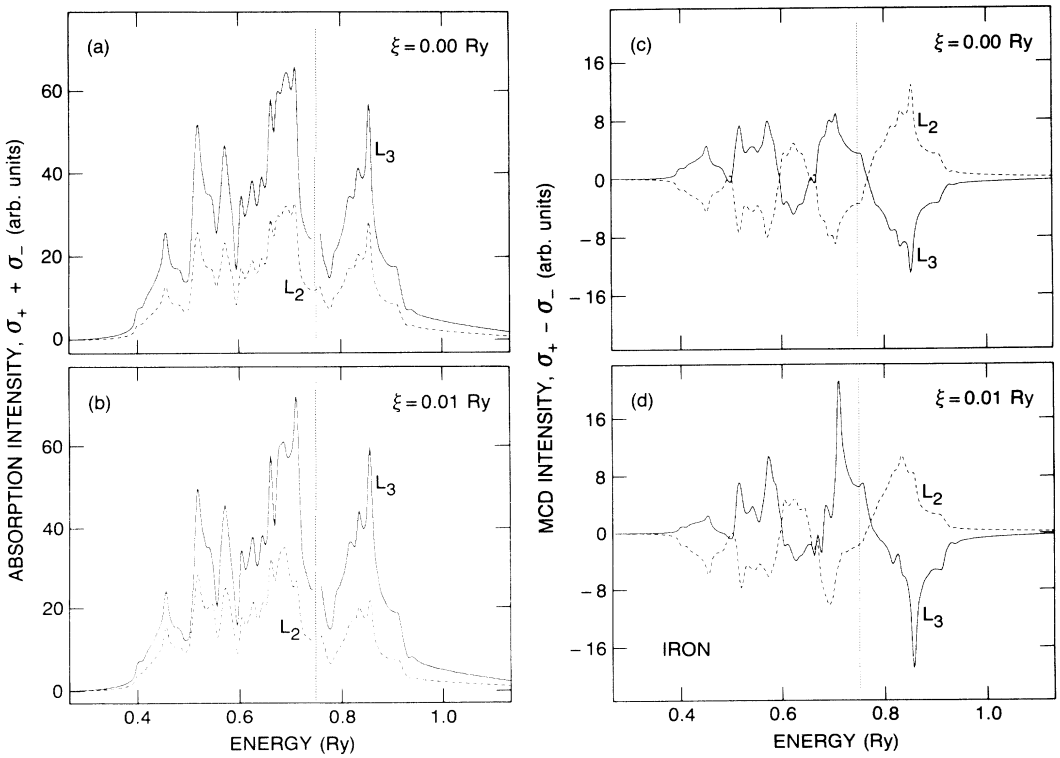

FIG. 5. Calculated L_3 (solid curves) and L_2 (dashed curves) spectra for Fe without regard for the exclusion principle. Panels (a) and (b) show the total absorption cross section $(\sigma_+ + \sigma_-)$ for $\xi=0$ and 0.01 Ry, respectively; panels (c) and (d) are the corresponding $(\sigma_+ - \sigma_-)$ MCD cross sections. The exchange parameters is $\Delta_{ex}=0.125$ Ry.

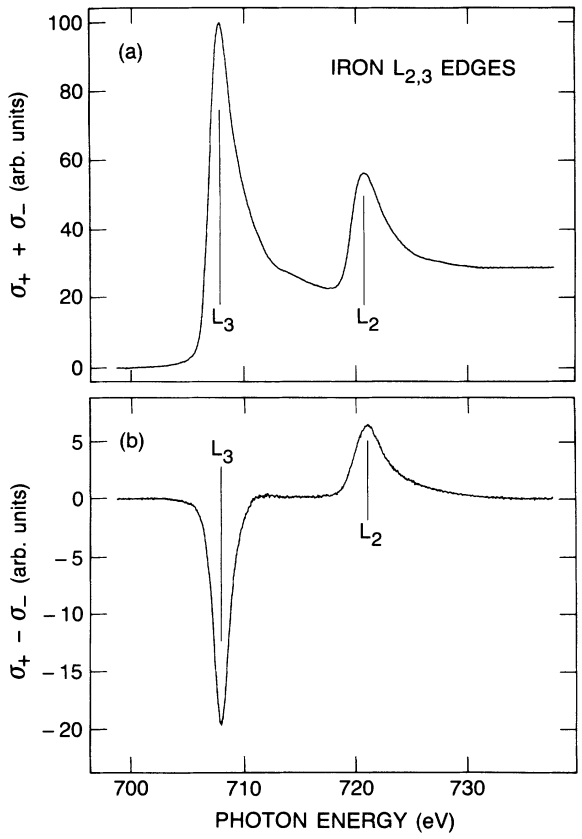

FIG. 6. Experimental data on Fe for (a) the total absorption cross section $(\sigma_+ + \sigma_-)$ and (b) the MCD cross section $(\sigma_+ - \sigma_-)$. The MCD spectrum shown here has been magnified by a factor 1.4 to account for incomplete photon polarization.

$\xi = 0.0053$ Ry.

In contrast with our experience on Ni, this value for ξ (or any other remotely plausible value) cannot account for the L_3- to L_2-intensity ratio in the Fe MCD $(\sigma_+ - \sigma_-)$ spectrum. This failure of the one-electron band picture is a consequence of the positive excursion of the calculated L_3 MCD signal at threshold. In the integrated intensity, this positive contribution annuls any increase in the negative contribution; thus the L_3- to L_2-MCD-intensity ratio cannot depart sufficiently from the Erskine-Stern value of $-1{:}1$.

C. Concluding discussion

We conclude that one-electron band theory fails in the description of the L_2 and L_3 edges of Fe. Only in the $(\sigma_+ + \sigma_-)$ spectrum can it work and then only by a large upward adjustment of ξ. The MCD $(\sigma_+ - \sigma_-)$ spectrum cannot be fixed in this way, thus affirming the desirability of both MCD and total absorption measurements. Another breakdown of our one-electron picture is the absence of structure in the measured spectra, even though the predicted structures are well within the available experimental resolution. This could be a many-body broadening effect due to the decay of the core hole. Although our results indicate the need for a many-body treatment, we do not find in the Fe MCD spectra the features B, B' which in Ni we have attributed to many-body effects.

It is interesting to note that the observed L_3- to L_2-intensity ratio in the MCD spectrum could be simulated if we were to allow ourselves another adjustable parameter. The failure of the MCD ratio to depart significantly from $-1{:}1$ is directly traceable to the appreciable positive excursion seen in Fig. 5 of the calculated L_3 MCD spectrum just above threshold. This difficulty could be removed by introducing E_F as a parameter and allowing it to move upward. Such an adjustment can be plausibly defended. The effect of core-hole creation would be to pull the d levels downward in energy (i.e., to make Fe look more like Co). We have not pursued this adjustment since it takes our model beyond its scope. The trend, however, looks correct. Along the same lines, we have noted earlier[11] that the value of ξ used in our optimal simulation for Ni is more characteristic of Cu than of Ni. We hope that these observations as well as the precision with which MCD spectra can be measured will stimulate future investigations by many-body theorists.

ACKNOWLEDGMENTS

We have benefited from our association with P. Carra, E. E. Chaban, Y. Ma, G. Meigs, and S. Modesti. One of us (N.V.S.) offers thanks to E. A. Stern for some indirect instruction in the matter of sum rules. The experimental data were taken at the National Synchrotron Light Source which is supported by the U.S. Department of Energy under Contract No. DE-AC0276CH00016.

[1]C. T. Chen, F. Sette, Y. Ma, and S. Modesti, Phys. Rev. B **42**, 7262 (1990); F. Sette, C. T. Chen, Y. Ma, S. Modesti, and N. V. Smith, in *X-ray Absorption Fine Structure*, edited by S. S. Hasnain (Horwood, New York, 1991).

[2]G. Schütz, W. Wagner, W. Wilhelm, P. Kienle, R. Zeller, R. Frahm, and G. Materlik, Phys. Rev. Lett. **58**, 737 (1987); G. Schütz, M. Knülle, R. Wienke, W. Wilhelm, W. Wagner, P. Kienle, and R. Frahm, Z. Phys. B **73**, 67 (1988); G. Schütz, R. Wienke, W. Wilhelm, W. Wagner, P. Kienle, R. Zeller, and R. Frahm, Z. Phys. **75**, 495 (1989); C. Kao, J. B. Hastings, E. D. Johnson, D. P. Siddons, G. C. Smith, and G. A. Prinz, Phys. Rev. Lett. **65**, 373 (1990).

[3]G. van der Laan, B. T. Thole, G. A. Sawatzky, J. B. Goedkoop, J. C. Fuggle, J.-M. Esteva, R. Karnatak, J. P. Remeika, and H. A. Dabkowska, Phys. Rev. B **34**, 6529 (1986); B. T. Thole, G. van der Laan, and G. A. Sawatzky, Phys. Rev. Lett. **55**, 2086 (1985).

[4]J. P. Hannon, G. T. Trammell, M. Blume, and D. Gibbs, Phys. Rev. Lett. **64**, 1286 (1990).

[5]E. Kisker, in *Polarized Electrons in Surface Physics*, edited by R. Feder (World Scientific, Singapore, 1985), p. 513.

[6]D. A. Papaconstantopoulos, *Handbook of the Band Structure of Elemental Solids* (Plenum, New York, 1986).

[7]M. Brown, R. E. Peierls, and E. A. Stern, Phys. Rev. B **15**, 738 (1977).

[8]G. D. Mahan, *Many-Particle Physics* (Plenum, New York,

1981).
[9]L. F. Mattheiss and R. E. Dietz, Phys. Rev. B **22**, 1663 (1980).
[10]See, for example, M. Schlüter and L. J. Sham, Phys. Rev. Lett. **51**, 1888 (1983).
[11]C. T. Chen, N. V. Smith, and F. Sette, Phys. Rev. B **43**, 6785 (1991).
[12]J. L. Erskine and E. A. Stern, Phys. Rev. B **12**, 5016 (1975).
[13]J. C. Slater and G. F. Koster, Phys. Rev. **94**, 1498 (1954).
[14]C. S. Wang and J. Callaway, Phys. Rev. B **9**, 4897 (1974).
[15]N. F. Mott, Proc. Phys. Soc. London A **62**, 416 (1949).
[16]E. U. Condon and G. H. Shortley, *Theory of Atomic Spectra* (Cambridge University Press, London, 1953); M. E. Rose, *Elementary Theory of Angular Momentum* (Wiley, New York, 1957).
[17]L. Hodges, H. Ehrenreich, and N. D. Lang, Phys. Rev. **152**, 505 (1966).
[18]J. Friedel, P. Lenglart, and G. Leman, J. Phys. Chem. Solids **25**, 781 (1964); E. Abate and M. Asdente, Phys. Rev. **140**, A1303 (1965).
[19]P. Weinberger and F. Rosicky, Theor. Chim. Acta **48**, 349 (1978).
[20]H. Ebert and R. Zeller, Phys. Rev. B **42**, 2744 (1990), and references therein.
[21]P. Carra and M. Alterelli, Phys. Rev. Lett. **64**, 1286 (1990).
[22]H. S. Bennett and E. A. Stern, Phys. Rev. **137**, A448 (1965).
[23]N. V. Smith, Adv. Phys. **16**, 629 (1967); E. A. Stern (private communication).
[24]C. E. Moore, *Atomic Energy Levels,* Natl. Bur. Stand. (U.S.) Circ. No. 467 (U.S. GPO, Washington, D.C., 1949), Vol. I; Vol. II (1952); Vol. III (1958).
[25]F. Herman and S. Skillman, *Atomic Structure Calculations* (Prentice-Hall, Englewood Cliffs, NJ, 1963).
[26]W. Eberhardt and E. W. Plummer, Phys. Rev. B **21**, 3245 (1980); F. J. Himpsel, J. A. Knapp, and D. E. Eastman, B **19**, 2919 (1979).
[27]D. J. Nagel, in *Band Structure Spectroscopy of Metals and Alloys,* edited by D. J. Fabian and L. M. Watson (Academic, New York, 1973), p. 457.
[28]L. A. Feldkamp and L. C. Davis, Phys. Rev. Lett. **43**, 151 (1979); L. C. Davis and L. A. Feldkamp, Solid State Commun. **34**, 141 (1980).
[29]J. Tersoff, L. M. Falicov, and D. R. Penn, Solid State Commun. **32**, 1045 (1979); D. R. Penn, Phys. Rev. Lett. **42**, 921 (1979).
[30]A. Liebsch, Phys. Rev. Lett. **43**, 1431 (1979); Phys. Rev. B **23**, 5203 (1981).
[31]G. Treglia, F. Ducastelle, and D. Spanjaard, Phys. Rev. B **21**, 3729 (1980).
[32]C. Guillot, Y. Ballu, J. Paigné, J. Lecante, K. P. Jain, P. Thiry, R. Pinchaux, Y. Petroff, and L. M. Falicov, Phys. Rev. Lett. **39**, 1632 (1977).
[33]R. Clauberg, W. Gudat, E. Kisker, E. Kuhlmann, and G. M. Rothberg, Phys. Rev. Lett. **47**, 1314 (1981).
[34]T. Jo and G. A. Sawatsky, Phys. Rev. B **43**, 8771 (1991).
[35]O. Eriksson, B. Johansson, R. C. Albers, A. M. Boring, and S. S. Brooks, Phys. Rev. B **42**, 2707 (1990), and references therein.
[36]M. Singh, C. S. Wang, and J. Callaway, Phys. Rev. B **11**, 287 (1975).

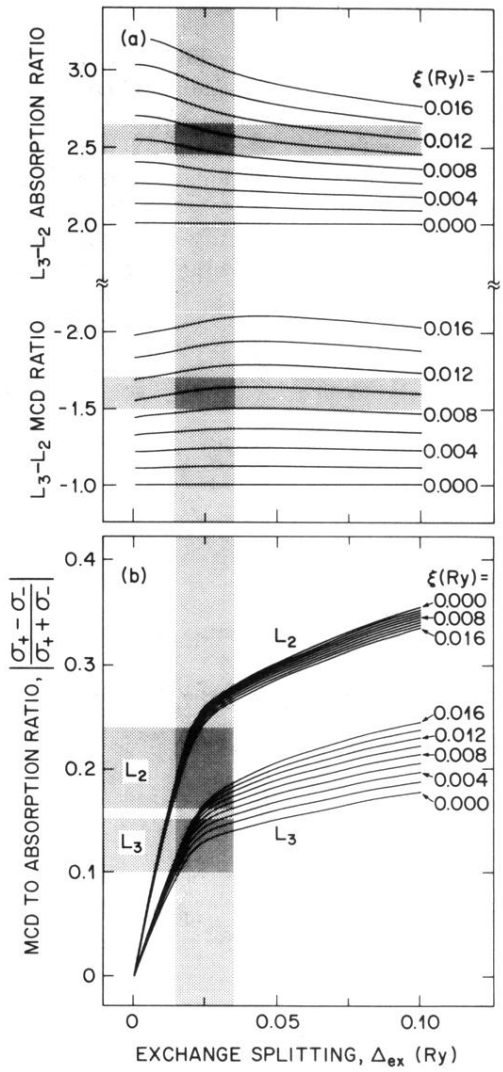

FIG. 2. Calculated intensity ratios of the L_2 and L_3 "white lines" of Ni as a function of the two key parameters ξ and Δ_{ex}: (a) *intraspectral* L_3 to L_2-intensity ratios and (b) *interspectral* ratios $(\sigma_+ - \sigma_-)/(\sigma_+ \sigma_-)$ for the individual L_2 and L_3 lines. Details of line-shape analysis are given in the text.